MAGNETIC FIELDS FROM THE PHOTOSPHERE TO THE CORONA
ASP Conference Series, Vol. 463
T. R. Rimmele, M. Collados Vera, et al., eds.

The Prominence/Coronal Cavity System: A Unified View of Magnetic Structures in the Solar Corona

T. Berger

Lockheed Martin Solar and Astrophysics Laboratory, Palo Alto, California, USA

Abstract. *Hinode*/SOT and SDO/AIA movies have given us new insights into the dynamic connections between prominences and coronal cavities. The observations suggest that prominences and coronal cavities are elements of a single large-scale structure in the solar corona: a helical magnetic flux rope. We discuss supporting observational evidence such as the relationship between the so-called "prominence bubbles" discovered by *Hinode*/SOT and coronal cavities, as well as spiral flows in the central regions of coronal cavities observed by AIA. We hypothesize that coronal cavity flux ropes support a form of magneto-thermal convection in which hot plasma and magnetic flux are transported upward into the coronal cavity flux rope with subsequent radiative cooling and condensation forming the partially ionized prominence return flows seen in visible light observations. Understanding the mass, magnetic flux, and helicity transport of this complex system will lead to better understanding of quiet Sun coronal mass ejections (CMEs).

1. Introduction

Prominences are formations of "chromospheric" plasma ($T \sim 10^4$ K, $n_e \sim 10^{17}$ m^3) found at heights in the solar atmosphere normally associated with the $T \sim 10^6$ K corona (Labrosse et al. 2010; Mackay et al. 2010). They form along large-scale "polarity inversion lines" (PIL) in the photospheric magnetic flux pattern. These regions are also called "filament channels" due to their effect on chromospheric topology (Martin 1998; Gaizauskas et al. 1997). Recent observations from the Solar Optical Telescope (SOT) (Tsuneta et al. 2008) on the Japanese/US/UK *Hinode* mission (Kosugi et al. 2007) have shown that prominences are highly dynamic structures supporting Alfvén waves (Okamoto et al. 2007), "bubbles" leading to Rayleigh-Taylor (RT) instabilities (Berger et al. 2011; Hillier et al. 2011; Berger et al. 2010; Hillier et al. 2010; Berger et al. 2008), and constant filamentary downflows (Berger et al. 2008; Chae et al. 2008; Haerendel & Berger 2011).

Coronal cavities are large (of order 100 Mm in scale) dark elliptical "voids" seen in white-light eclipse and EUV coronal images, typically at heliographic latitudes above 40 degrees (Saito & Hyder 1968). They underlie "arcade" field lines which transition with height to long "helmet streamer" structures extending radially outward to many solar radii (Saito & Tandberg-Hanssen 1973). Coronal cavities are dark due to a $\sim 30 - 40\%$ density deficit relative to the surrounding arcade (Vásquez et al. 2009; Fuller & Gibson 2009). The temperature in cavities may be elevated relative to the surrounding arcade loops (Vásquez et al. 2009; Fuller & Gibson 2009; Guhathakurta et al.

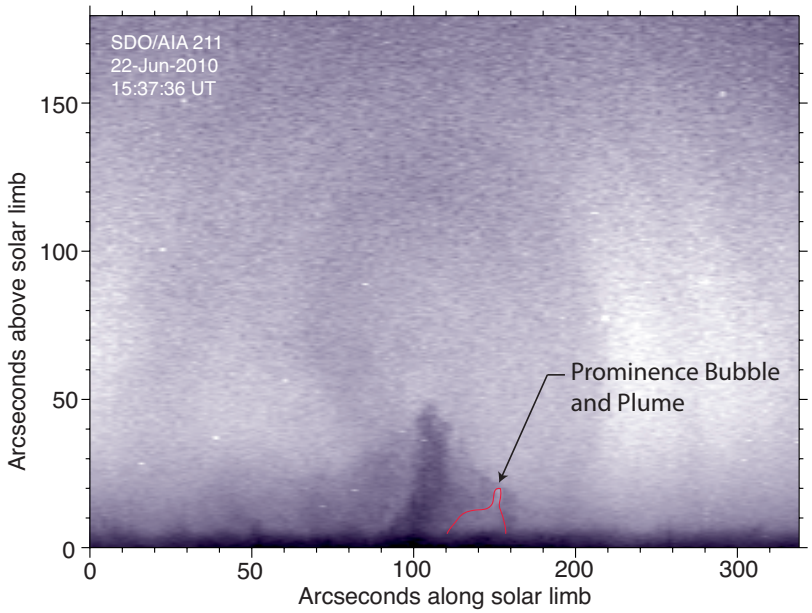

Figure 1. Large coronal cavity and quiescent prominence seen in the SDO/AIA 211 channel on the NW limb on 22-June-2010. The image has been transformed to polar $r-\theta$ coordinates. An arctangent contrast transform has been applied to enhance the above-limb structure and a square-root color table has been applied. Note that the center region of the cavity directly above the prominence is brighter than the outer regions of the cavity. A large prominence bubble and plume event is outlined in red. This event is analyzed in Berger et al. (2011).

1999), but it is not yet clear if this is due to sub-structure (e.g., hotter cores) within the cavity. Recent doppler shift measurements (Schmit et al. 2009) and observations of rotational motions (Wang & Stenborg 2010) show that coronal cavities can support complex flows. Models of coronal cavities show that their properties are consistent with helical magnetic flux ropes anchored above photospheric PILs (Gibson et al. 2010). Not all coronal cavities have associated prominences, but nearly all quiescent polar crown prominences show observable coronal cavities at some point in their evolution. The importance of coronal cavities lies in the fact that they form the bulk of quiet-Sun CMEs, accounting for $\sim 40\%$ of all solar eruptions (Gopalswamy 2006; Pevtsov et al. 2012).

With the launch of *Hinode*/SOT and SDO/AIA (Lemen et al. 2012) we have for the first time two high-resolution instruments capable of showing the full range of prominence plasma dynamics (*Hinode*/SOT) simultaneously with the dynamics of the overlying coronal cavity (SDO/AIA). The 211 Å channel of AIA shows coronal cavities above the limb particularly well, while the 171 Å and 304 Å channels of AIA reveal emission in the "prominence/corona transition region" (PCTR, Parenti & Vial 2007).

2. Observations of prominences and coronal cavities

Figure 1 shows an SDO/AIA 211 channel image of a large quiescent prominence and its associated coronal cavity on the western solar limb. Three things of note in this im-

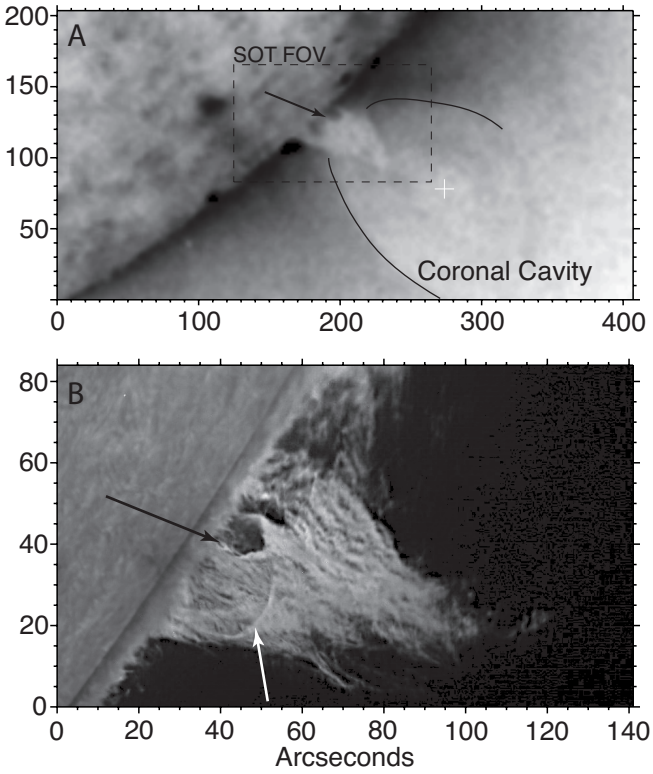

Figure 2. *Top*, **a**: STEREO-B/EUVI (negative) image of a large coronal cavity and its associated quiescent prominence. The white cross marks the approximate center of the cavity approximately 150″ above the limb. The black arrow indicates a large prominence bubble event. The *Hinode*/SOT field-of-view is indicated by the black dashed rectangle. *Bottom*, **b**: *Hinode*/SOT Hα image of the quiescent prominence seen in *panel A*. The large bubble event is indicated by the black arrow. The white arrow points out another bubble event that was obscured by foreground prominence emission.

age are (1) the highest portion of the prominence "spine" reaches well into the cavity, (2) the region directly above the prominence is somewhat brighter than the surrounding cavity, and (3) a "prominence bubble" and plume event are seen on the right hand side of the prominence. Brighter "chewy nougat" central regions have been noted in earlier cavity studies (Hudson et al. 1999). However with the high temporal cadence of AIA we can now see that these bright central regions harbor complex motions. In the cavity shown in Figure 1 the bright plasma appears at times to be moving upwards from the prominence into the cavity while also oscillating in a "swaying mode" of several minutes period along with the bulk of the prominence plasma below. Prominence bubbles are large dark (in visible light) inclusions that rise from the chromosphere, eventually triggering the RT instability in the prominence (Hillier et al. 2011; Berger et al. 2010). They have been seen in rare ground-based Hα observations (de Toma et al. 2008; Stellmacher & Wiehr 1973) but are most easily detectable in *Hinode*/SOT and SDO/AIA movies. Multi-instrument analyses show that the plasma in prominence bubbles is low density (Heinzel et al. 2008) compared to the surrounding prominence and heated to

temperatures from 250,000 K to 1 MK (Berger et al. 2011). A movie of this prominence/cavity combination is available online[1].

Figure 2a shows the relationship between another large quiescent prominence to the overlying coronal cavity. As in Figure 1, a prominence bubble can be seen in its early formation stage. The bubble shown in Figure 2 eventually travelled completely through the prominence with a speed of about 20-25 km s^{-1} (Berger et al. 2010; Schmieder et al. 2010). The bubble is large enough to be visible in the STEREO-B/EUVI image in Figure 2a with a projected diameter of approximately 10″ . The minor axis diameter of the overlying elliptical coronal cavity is approximately 150 arcseconds, showing that the prominence bubble is a non-negligible fraction of the cavity size. *Hinode*/SOT observations (Okamoto et al. 2010, 2008) suggest that prominence bubbles are caused by emerging magnetic flux. Since prominence bubbles recur on time scales of hours, they may represent a significant cumulative source of coronal cavity magnetic flux.

A movie of SDO/AIA data taken on 05-May-2010 [2] shows a large coronal cavity at the southwest limb with plasma injected into the center of the cavity by a nearby filament activation event. The motion of the plasma is along the cavity axis with an obvious spiraling component. An interesting aspect of this event is that the original material injected into the cavity is chromospheric filament plasma (seen as dark material in the AIA 211 channel) presumably at a temperature of $\sim 10^4$ K. However as the material flows into the central axis region of the cavity it heats enough to switch to emission in AIA 211. This implies that the plasma temperature is in excess of 1 MK, apparently heated by some mechanism related to the flow into the cavity. Given that plasma is fully ionized at this temperature, the subsequent spiral motion must therefore be due to flow along helical magnetic field lines in the center of the cavity.

Finally, Figure 3 shows another peculiar phenomenon discovered in AIA prominence observations: curved extensions of coronal plasma leading from the upper regions of the quiescent prominence into the overlying coronal cavity. The nature of these "horns" of coronal plasma remains unexplained. In particular it is not known whether the plasma in these extensions is in motion and if so, whether it is flowing down from the cavity into the prominence or in the opposite direction. These horns are a common, if not ubiquitous, feature of all quiescent prominences observed with the AIA instrument, best viewed in the 171 channel which images plasma in the 800,000 K – 10^6 K range. They are sometimes clearly observed in quiet-Sun CME events (e.g., Régnier et al. 2011).

In summary, the combination of *Hinode*/SOT and SDO/AIA has led to the discovery of several new aspects of the prominence/coronal cavity relationship, namely

- Prominence bubbles and the associated RT instability flows: a mechanism by which hot plasma is transported from the photosphere into coronal cavities.
- Spiral flows: intermittent flows of plasma along helical trajectories in the central "chewy nougat" regions of coronal cavities.
- Prominence "horns": coronal plasma curving from the upper regions of prominences upwards into the coronal cavity above.

---

[1] `http://www.lmsal.com/berger/public/ATST-EAST/ATST-EAST_Berger_Fig1.mov`

[2] `http://www.lmsal.com/berger/public/ATST-EAST/ATST-EAST_Berger_corkscrew.mov`

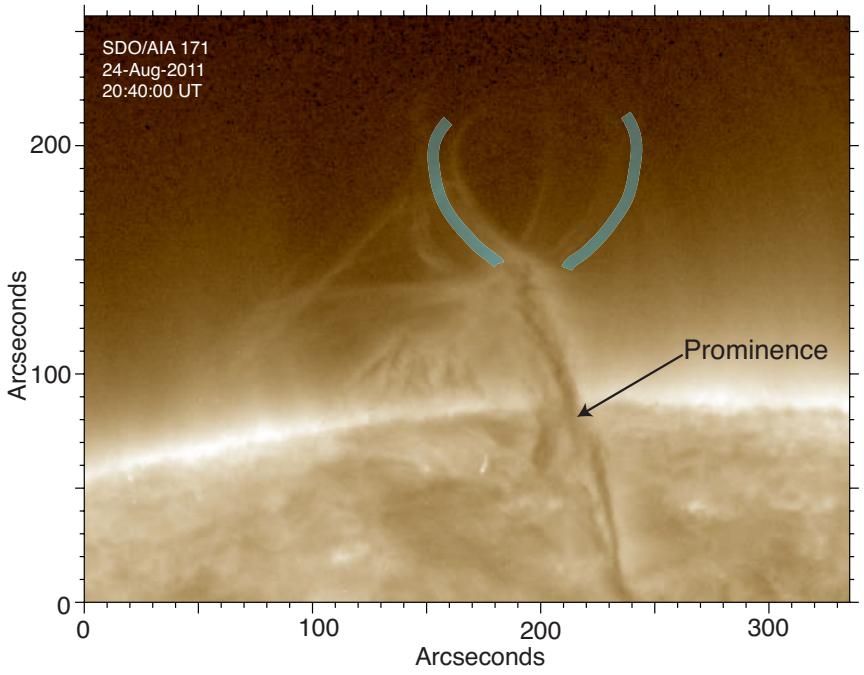

Figure 3. Large quiescent prominence seen in SDO/AIA 171 channel on the SW limb on 24-Aug-2011. The prominence is visible in absorption while large "horns" in emission protrude from the top region of the prominence into the coronal cavity above. The translucent blue curves highlight the path of the horns which are 50″ – 75″ in length (sky projection).

3. The helical flux rope hypothesis

The items discussed in Section 2 can be understood as elements of a single magnetic structure in the solar corona: the helical magnetic flux rope. In this view, the flux rope central region is evacuated by magnetic pressure to create the large-scale coronal cavity seen in EUV and white light images. Measurements of quiescent prominence magnetic fields (Casini et al. 2003; Bommier et al. 1994) show that the majority of them have so-called "inverse polarity" configurations that are consistent with flux rope models (e.g., Kuperus & Raadu 1974).

The spiral flows observed in the center of coronal cavities offer strong evidence that the magnetic field lines in cavities have helical topology. Plasma injected into this region becomes trapped on the helical field lines to form the brighter central emission often seen in coronal cavities. As the cavity plasma radiatively cools and neutralizes, it descends to the current sheet region where the magnetic field is weak and chaotic (van Ballegooijen & Cranmer 2010), eventually forming a prominence. Quiescent prominence filamentary downflows are a natural result of low-ionization state plasma flowing under gravity in the complex topology of the current sheet region. Since the current sheet region supports a constant slow reconnection of field lines there must be an inflow of the surrounding coronal plasma into the region. The "horns" noted in most AIA

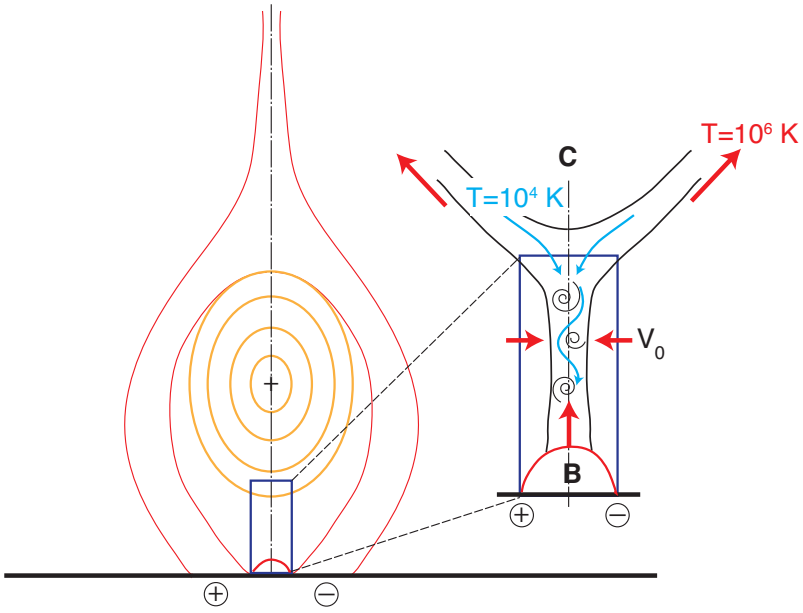

Figure 4. Schematic of proposed coronal cavity/prominence flux rope model. *Left*: the coronal cavity flux rope is shown as the gold elliptical magnetic field contours below red arcade and helmet streamer field lines. The blue rectangle encloses the prominence formation/current sheet region below the flux rope. *Right*: enlargement of the current sheet region showing a prominence bubble (denoted "B') as a proposed magnetic flux emergence across the PIL rising into the current sheet region above. The current sheet region is characterized by chaotic and weak magnetic fields. Blue arrows indicate chromospheric (10^4 K) partially ionized plasma falling into the current sheet after radiatively cooling in the cavity above (denoted by "C"). Coronal plasma surrounding the prominence/current sheet flows into the system at a characteristic reconnection speed of V_0. Hot coronal plasma is depicted being transported up along field lines outlining the bottom of the flux rope, the so-called "horns" noted in Section 2.

171 observations of prominences may be formed as this flow is redirected upwards by reconnection. Finally, prominence bubbles can be understood as emerging flux events that happen to take place directly underneath the flux rope, across the PIL, and are thus revealed by subsequent RT instability flows as they rise into the cool prominence in the current sheet region above. Figure 4 shows a schematic of our proposed configuration based on earlier models (van Ballegooijen & Cranmer 2010; Malherbe & Priest 1983; Kuperus & Raadu 1974).

4. Coronal condensation, convection, and the evolution to eruptive states

The central concept linking prominences to cavities in this hypothesis is that of coronal condensation: the source of the weakly ionized plasma in quiescent prominences is condensation from hot plasma that has radiatively cooled in the cavity region above. Observations of coronal cavities without an associated prominence are understood as cavities with insufficient internal plasma to support significant prominence formation.

Conversely, in this model if there is a quiescent prominence then there *must* be an associated flux rope above it; observations of prominences without associated coronal cavities are explained as line-of-sight effects in which the cavity is occluded by foreground arcade emission (Gibson et al. 2010). In support of this concept, coronal condensation leading to prominence formation has now been seen in several AIA observations, particularly following CME events where presumably a large amount of plasma passes through the corona with some residual amount ending up in nearby flux ropes (e.g., Liu et al. 2012).

Prominence formation by coronal condensation was dismissed based on early comparisons of coronal and prominence densities (Saito & Tandberg-Hanssen 1973). But this argument assumes a static corona, i.e., *at any one time* the total mass of plasma in the corona is insufficient to supply the observed mass of more than a few prominences. However observations show that the prominence/coronal cavity system is not static. Thus as long as the mass injection rate into the flux rope is at least equal to the mass drainage rate in the prominence, an equilibrium state can be achieved in which long-lived coronal cavities with associated draining prominences can exist.

In this picture, coronal flux ropes represent efficient "traps" in the solar atmosphere where any plasma finding its way into the system is efficiently suspended in the corona and can only slowly escape to the lower atmosphere through the current sheet region[3], thus forming long-lived prominences in the process. In contrast, "coronal rain" is plasma trapped on simple loop field lines that offer little suspension and thus rapidly transport the plasma downwards at speeds approaching free-fall velocities (Schrijver 2001).

Thus we conjecture that coronal cavity flux ropes support a form of "coronal convection" in which hot plasma is injected into the flux rope through various mechanisms (e.g., CMEs (Liu et al. 2012), prominence bubble events (Berger et al. 2011), footpoint thermal flows (Karpen & Antiochos 2008; Xia et al. 2011), spicules (De Pontieu et al. 2011), etc.) and radiatively cools to eventually condense into a prominence in the current sheet below the flux rope. The prominence plasma then drains back to the lower atmosphere through the filamentary downflows at speeds of ~ 10 km s^{-1}. Theoretical investigations of plasma radiative cooling and cross-field transport to form prominence accumulations are currently ongoing (Low et al. 2012, in preparation).

Of particular note in this proposed system is the role of the prominence bubble events. If the hypothesis that these bubbles are magnetic flux emergence events proves correct, then the bubbles represent a mechanism by which not only hot plasma but magnetic flux and helicity are transported via the RT instability into overlying coronal flux ropes. Numerical simulations (Hillier et al. 2011) show that while the net mass flux due to the RT instability is downward, the net magnetic flux transport is upwards. Other studies (Zhang et al. 2006; Gibson et al. 2004) have shown that buildup of magnetic flux and helicity in large-scale coronal flux ropes drives a quasi-steady evolution of the system towards an eruptive state in which the magnetic buoyancy overcomes the tension forces of the overlying arcade fields. Thus we have a consistent picture based on observations in which magnetic flux emergence and transport leads to gradual accumulation of flux and eventual destabilization of the flux rope, culminating in a quiet Sun CME.

---

[3]Plasma in the flux rope could presumably also drain along the end-point field lines of the flux rope that anchor to the photosphere, but these are quite distant from most of the tube interior volume.

5. Summary

We have examined several new aspects of quiescent prominences and coronal cavities discovered in *Hinode*/SOT and SDO/AIA observations. The observations can be consistently understood as elements of a single magnetic structure in the solar corona: the large-scale helical magnetic flux rope. Based on the longitudinal extent of observed filaments and coronal cavities these magnetic structures are by far the largest coherent magnetic structures on the Sun, sometimes spanning up to 120 degrees in heliographic longitude (as in the recent Nov-Dec 2011 event).

Our hypothesis can be further tested by observations to establish the magnetic nature of prominence bubble events. *Hinode*/SOT or the SDO/HMI instrument with concurrent AIA 304 observations may prove capable of this observation. However a higher resolution telescope with a simultaneous magnetic and Hα filament/prominence imaging instruments would be better suited. The ATST Visible Specropolarimeter (ViSP) combined with the Visible Broadband Imager (VBI) and Visible Tunable Filter (VTF) instruments will be an ideal combination for this study. In addition, direct measurements of prominence and cavity magnetic fields are needed. These measurements will likely require a dedicated space-based instrument suite such as the recently proposed Solar-C mission.

References

Berger, T., Testa, P., Hillier, A., Boerner, P., Low, B. C., Shibata, K., Schrijver, C., Tarbell, T., & Title, A. 2011, Nat, 472, 197

Berger, T. E., Shine, R. A., Slater, G. L., Tarbell, T. D., Title, A. M., Okamoto, T. J., Ichimoto, K., Katsukawa, Y., Suematsu, Y., Tsuneta, S., Lites, B. W., & Shimizu, T. 2008, ApJ, 676, L89

Berger, T. E., Slater, G., Hurlburt, N., Shine, R., Tarbell, T., Title, A., Lites, B. W., Okamoto, T. J., Ichimoto, K., Katsukawa, Y., Magara, T., Suematsu, Y., & Shimizu, T. 2010, ApJ, 716, 1288

Bommier, V., Landi Degl'Innocenti, E., Leroy, J.-L., & Sahal-Brechot, S. 1994, Solar Phys., 154, 231

Casini, R., López Ariste, A., Tomczyk, S., & Lites, B. W. 2003, ApJ, 598, L67

Chae, J., Ahn, K., Lim, E.-K., Choe, G. S., & Sakurai, T. 2008, ApJ, 689, L73

De Pontieu, B., McIntosh, S. W., Carlsson, M., Hansteen, V. H., Tarbell, T. D., Boerner, P., Martinez-Sykora, J., Schrijver, C. J., & Title, A. M. 2011, Science, 331, 55

de Toma, G., Casini, R., Burkepile, J. T., & Low, B. C. 2008, ApJ, 687, L123

Fuller, J., & Gibson, S. E. 2009, ApJ, 700, 1205

Gaizauskas, V., Zirker, J. B., Sweetland, C., & Kovacs, A. 1997, ApJ, 479, 448

Gibson, S. E., Fan, Y., Mandrini, C., Fisher, G., & Demoulin, P. 2004, ApJ, 617, 600

Gibson, S. E., Kucera, T. A., Rastawicki, D., Dove, J., de Toma, G., Hao, J., Hill, S., Hudson, H. S., Marqué, C., McIntosh, P. S., Rachmeler, L., Reeves, K. K., Schmieder, B., Schmit, D. J., Seaton, D. B., Sterling, A. C., Tripathi, D., Williams, D. R., & Zhang, M. 2010, ApJ, 724, 1133

Gopalswamy, N. 2006, Journal of Astrophysics and Astronomy, 27, 243

Guhathakurta, M., Fludra, A., Gibson, S. E., Biesecker, D., & Fisher, R. 1999, Journal of Geophysical Research, 104, 9801

Haerendel, G., & Berger, T. 2011, ApJ, 731, 82

Heinzel, P., Schmieder, B., Fárník, F., Schwartz, P., Labrosse, N., Kotrč, P., Anzer, U., Molodij, G., Berlicki, A., DeLuca, E. E., Golub, L., Watanabe, T., & Berger, T. 2008, ApJ, 686, 1383

Hillier, A., Isobe, H., Shibata, K., & Berger, T. 2011, ApJ, 736, L1

Hillier, A., Shibata, K., & Isobe, H. 2010, PASJ, 62, 1231
Hudson, H. S., Acton, L. W., Harvey, K. L., & McKenzie, D. E. 1999, ApJ, 513, L83
Karpen, J. T., & Antiochos, S. K. 2008, ApJ, 676, 658
Kosugi, T., Matsuzaki, K., Sakao, T., Shimizu, T., Sone, Y., Tachikawa, S., Hashimoto, T., Minesugi, K., Ohnishi, A., Yamada, T., Tsuneta, S., Hara, H., Ichimoto, K., Suematsu, Y., Shimojo, M., Watanabe, T., Shimada, S., Davis, J. M., Hill, L. D., Owens, J. K., Title, A. M., Culhane, J. L., Harra, L. K., Doschek, G. A., & Golub, L. 2007, Solar Phys., 243, 3
Kuperus, M., & Raadu, M. A. 1974, A&A, 31, 189
Labrosse, N., Heinzel, P., Vial, J.-C., Kucera, T., Parenti, S., Gunár, S., Schmieder, B., & Kilper, G. 2010, Space Sci.Rev., 151, 243
Lemen, J. R., Title, A. M., Akin, D. J., Boerner, P. F., Chou, C., Drake, J. F., Duncan, D. W., Edwards, C. G., Friedlaender, F. M., Heyman, G. F., Hurlburt, N. E., Katz, N. L., Kushner, G. D., Levay, M., Lindgren, R. W., Mathur, D. P., McFeaters, E. L., Mitchell, S., Rehse, R. A., Schrijver, C. J., Springer, L. A., Stern, R. A., Tarbell, T. D., Wuelser, J.-P., Wolfson, C. J., Yanari, C., Bookbinder, J. A., Cheimets, P. N., Caldwell, D., Deluca, E. E., Gates, R., Golub, L., Park, S., Podgorski, W. A., Bush, R. I., Scherrer, P. H., Gummin, M. A., Smith, P., Auker, G., Jerram, P., Pool, P., Soufli, R., Windt, D. L., Beardsley, S., Clapp, M., Lang, J., & Waltham, N. 2012, Solar Phys., 275, 17
Liu, W., Berger, T. E., & Low, B. C. 2012, ApJ, 745, L21
Mackay, D. H., Karpen, J. T., Ballester, J. L., Schmieder, B., & Aulanier, G. 2010, Space Sci.Rev., 151, 333
Malherbe, J. M., & Priest, E. R. 1983, A&A, 123, 80
Martin, S. F. 1998, Solar Phys., 182, 107
Okamoto, T. J., Tsuneta, S., & Berger, T. E. 2010, ApJ, 719, 583
Okamoto, T. J., Tsuneta, S., Berger, T. E., Ichimoto, K., Katsukawa, Y., Lites, B. W., Nagata, S., Shibata, K., Shimizu, T., Shine, R. A., Suematsu, Y., Tarbell, T. D., & Title, A. M. 2007, Science, 318, 1577
Okamoto, T. J., Tsuneta, S., Lites, B. W., Kubo, M., Yokoyama, T., Berger, T. E., Ichimoto, K., Katsukawa, Y., Nagata, S., Shibata, K., Shimizu, T., Shine, R. A., Suematsu, Y., Tarbell, T. D., & Title, A. M. 2008, ApJ, 673, L215
Parenti, S., & Vial, J.-C. 2007, A&A, 469, 1109
Pevtsov, A. A., Panasenco, O., & Martin, S. F. 2012, Solar Phys., 277, 185
Régnier, S., Walsh, R. W., & Alexander, C. E. 2011, A&A, 533, L1
Saito, K., & Hyder, C. L. 1968, Solar Phys., 5, 61
Saito, K., & Tandberg-Hanssen, E. 1973, Solar Phys., 31, 105
Schmieder, B., Chandra, R., Berlicki, A., & Mein, P. 2010, A&A, 514, A68
Schmit, D. J., Gibson, S. E., Tomczyk, S., Reeves, K. K., Sterling, A. C., Brooks, D. H., Williams, D. R., & Tripathi, D. 2009, ApJ, 700, L96
Schrijver, C. J. 2001, Solar Phys., 198, 325
Stellmacher, G., & Wiehr, E. 1973, A&A, 24, 321
Tsuneta, S., Ichimoto, K., Katsukawa, Y., Nagata, S., Otsubo, M., Shimizu, T., Suematsu, Y., Nakagiri, M., Noguchi, M., Tarbell, T., Title, A., Shine, R., Rosenberg, W., Hoffmann, C., Jurcevich, B., Kushner, G., Levay, M., Lites, B., Elmore, D., Matsushita, T., Kawaguchi, N., Saito, H., Mikami, I., Hill, L. D., & Owens, J. K. 2008, Solar Phys., 249, 167
van Ballegooijen, A. A., & Cranmer, S. R. 2010, ApJ, 711, 164
Vásquez, A. M., Frazin, R. A., & Kamalabadi, F. 2009, Solar Phys., 256, 73
Wang, Y.-M., & Stenborg, G. 2010, ApJ, 719, L181
Xia, C., Chen, P. F., Keppens, R., & van Marle, A. J. 2011, ApJ, 737, 27
Zhang, M., Flyer, N., & Low, B. C. 2006, ApJ, 644, 575